

Catastrophe Observation in a Josephson-Junction System

M. G. Castellano,¹ F. Chiarello,¹ R. Leoni,¹ F. Mattioli,¹ G. Torrioli,¹ P. Carelli,² M. Cirillo,³ C. Cosmelli,⁴ A. de Waard,⁵ G. Frossati,⁵ N. Grønbech-Jensen,⁶ and S. Poletto⁷

¹*Istituto di Fotonica e Nanotecnologie del CNR and INFN, 00156 Roma, Italy*

²*Dipartimento di Ingegneria Elettrica and INFN, Università dell'Aquila, 67040 L'Aquila, Italy*

³*Dipartimento di Fisica and INFN, Università di Roma Tor Vergata, 00173 Roma, Italy*

⁴*Dipartimento di Fisica and INFN, Università di Roma La Sapienza, 00195 Roma, Italy*

⁵*Kamerlingh Onnes Laboratory, Leiden University, 2333 CA Leiden, The Netherlands*

⁶*Department of Applied Science, University of California, Davis, California 95616, USA*

⁷*Dipartimento di Fisica and INFN, Università di Roma Tre, 00146 Roma, Italy*

(Received 2 September 2006; published 25 April 2007)

We report on experiments performed to probe quantum coherence in a system consisting of an rf-SQUID in which the Josephson junction is replaced by a small loop containing two junctions in parallel. At temperatures of the order of 10 mK the system may develop three potential energy wells, which modify the usual two well energy profile and thereby verify the qubit manipulation strategy. The appearance of the third potential well can be interpreted as evidence of a butterfly catastrophe, namely, a catastrophe expected for a system described by four control parameters and one state variable.

DOI: 10.1103/PhysRevLett.98.177002

PACS numbers: 85.25.Cp, 05.45.-a, 74.50.+r

Since the pioneering work by Leggett and Garg [1], the observation of quantum behavior of macroscopic superconducting variables has renewed the attention toward Josephson systems and superconducting quantum interference devices (SQUIDs). The response and dynamics of systems consisting of single [2] or coupled [3] Josephson junctions and interferometers [4] have been proposed and investigated in order to understand the nature of fundamental states and transitions between them. The acquired knowledge has been exploited in the growing field of quantum information processing with solid state devices [5]. In this framework, we have engineered a system that requires no external microwave pumping in order to provide evidence of quantum coherence.

We study the properties of the system whose electrical analogue is sketched in Fig. 1(a): it consists in essence of a double-SQUID; namely, a superconducting loop with inductance L interrupted by a small dc-SQUID with inductance l . When the effect of the small inductance l can be neglected the inner dc-SQUID can be viewed as a single Josephson junction with tunable critical current, and the potential energy of the system has the form of the corrugated parabola of an rf-SQUID. This potential can be tilted by the applied flux Φ_x [Fig. 1(b)] and manipulated through the flux Φ_c , which can lower the barrier [Fig. 1(c)]. The states in the right and left well of Figs. 1(b) and 1(c) correspond to clockwise and counterclockwise current polarization states of the large loop.

When the barrier of the potential well is very low and the temperature of the system is well below the expected quantum to classical crossover temperature [2] one can expect coherent oscillations between these two polarization states. These states are read out either by a hysteretic dc-SQUID, coupled through a superconducting trans-

former, or by a larger Josephson junction [6], inserted into the double-SQUID loop [Fig. 1(a)].

In Fig. 2(a) we show a typical total flux vs control flux Φ_x characteristics, taken at 10 mK on our double SQUID with a fixed value of the control flux Φ_c . We see that the characteristics are essentially those of an rf-SQUID [7]; however, tuning the height of the potential barrier, which can be achieved just by varying the flux Φ_c , will result in a reduction or enlargement of the hysteresis cycle. Recording the characteristics of Fig. 2(a) for different values of the flux Φ_c we will obtain the separatrix for the potential energy configurations in the (Φ_x, Φ_x) -plane as shown in Fig. 2(b). We found the plane of Fig. 2(b) to be a physically relevant and versatile tool to characterize the device be-

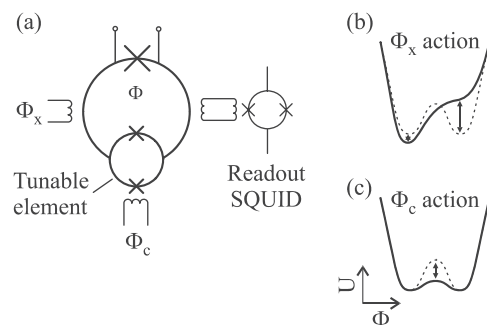


FIG. 1. (a) The double-SQUID system whose configurations and stability are investigated in the Letter. The switching between flux states, induced by the fluxes Φ_x and Φ_c , can be recorded through the readout junction or through the readout SQUID. Examples of the control of the system potential through Φ_x and Φ_c are given in (b) and (c), respectively: the first modifies the symmetry while the second tunes the height of the barrier.

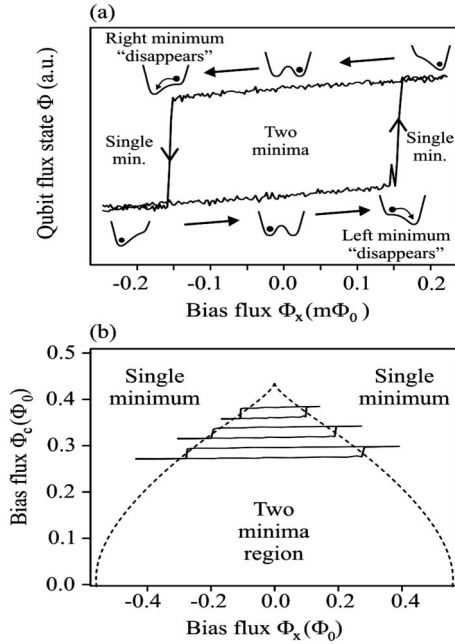


FIG. 2. (a) An experimental flux characteristic of the double-SQUID system for a fixed value of Φ_c where we also report for every region of the curve the potential configuration. (b) A diagram of the potential configuration in the (Φ_x, Φ_c) -plane, obtained by plotting the positions at which the two minima disappear. For clarity, we superimpose the characteristics shown in (a) taken for various values of Φ_c .

havior. In particular, the tip of the map is the most important region for our investigations because here the height of the potential barrier between the two wells attains very low values, and, thus, where we can expect evidence of quantum coherence from the occupation statistics histograms.

In Fig. 3 we show the experimental data (open circles) corresponding to the map sketched in Fig. 2(b). Figure 3(a) shows that the tip is bending on the left; the detail of the very top, within the dotted square, is enlarged in Fig. 3(b).

The shape of the flux characteristics for $\Phi_c \equiv \Phi_0/2$ can be fitted and provides information on the physical parameters of the inner dc-SQUID junctions. The data plotted in Fig. 3(a) indicate an asymmetry of about 4% between the critical currents of the junctions forming the inner junction loop. We attribute this asymmetry to flux trapped in the junctions because improving the shielding of the samples results in more symmetrical flux characteristics (estimated asymmetry of about 0.3%) and the backbending of Fig. 3(a) disappears. However, instead of the backbending we now observe “two-horns” on the tip shown in Fig. 3(c). Unfortunately, both patterns in Fig. 3(a) and the more symmetrical one in Fig. 3(c) are disturbing factors for our quantum coherence experiments because they indicate a modified shape of the potential in the lowest barrier region: in order to understand this phenomenon we put the observations into the following context.

The inner dc-SQUID contributes additional complexity to the potential energy function when the inductance l of

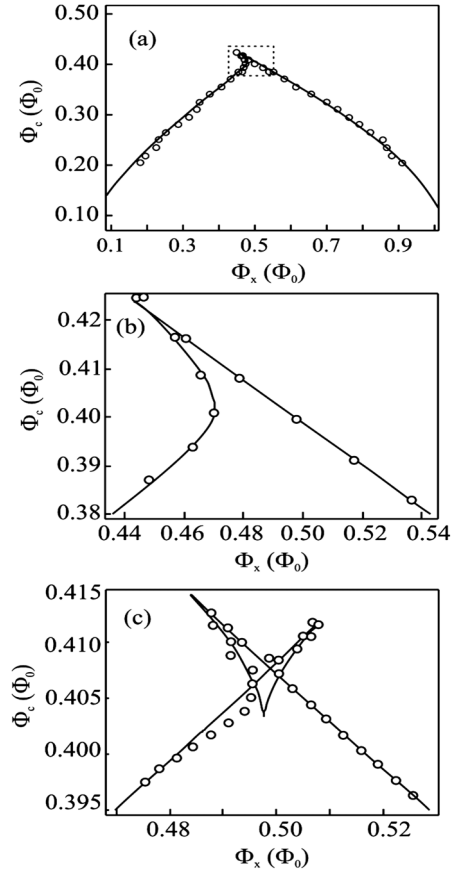


FIG. 3. Experimental Φ_x - Φ_c phase diagram obtained for two different asymmetry parameters determining the value of the coefficient to the third order power coefficient in Eq. (3). (a) Difference between the critical currents is 4%. (b) Enlargement of the tip region. Continuous line is the theoretical expression while the circles are the experimental points. (c) Butterfly catastrophe observed by enlarging the tip of the map when the coefficient to the third order in Eq. (3) is close to zero (asymmetry of 0.3%).

the inner loop of Fig. 1(a) cannot be neglected. With the phase differences between the quantum mechanical wave functions in the inner loop denoted by φ_1 and φ_2 , it can be shown that the system can be described by the single variable $\varphi = (\varphi_1 + \varphi_2)/2$ in the limit $l \ll L$. The approximate potential energy function reads [8]

$$U = \frac{1}{2}E_L(\varphi - \varphi_x)^2 - E_S \cos \varphi + E_D \sin \varphi - \frac{1}{2}E_I \cos^2 \varphi, \quad (1)$$

where $\Phi_0 = 2.07 \times 10^{-15}$ Wb is the magnetic flux quantum, $\varphi_x = 2\pi\Phi_x/\Phi_0$ and there are four energy scales. The first, $E_L = \Phi_0^2/(4\pi^2L)$, is related to the magnetic energy stored in the main loop, while $E_S = E_{S0} \cos(\pi\Phi_c/\Phi_0)$, $E_D = E_{D0} \sin(\pi\Phi_c/\Phi_0)$, and $E_I = E_{I0} \sin^2(\pi\Phi_c/\Phi_0)$ represent, respectively, the harmonic modulations (through the applied flux Φ_c) of $E_{S0} = (I_{C1} + I_{C2})\Phi_0/(2\pi)$ (maximum Josephson energy of the two junctions of the internal loop), $E_{D0} = (I_{C1} - I_{C2})\Phi_0/(2\pi)$ (Josephson energy due to the difference of the critical currents) and $E_{I0} = (I_{C1} + I_{C2})^2 l/4$ (energy stored in the inductor l). Thus, Eq. (1) describes the potential energy of the system by one vari-

able, and four characteristic energies. Starting from Eqs. 1 and 2 of Ref. [8] (with no noise current terms) but setting different Josephson currents (I_{C1} and I_{C2}) for the junctions of the inner loop one derives the following equation (analogous to Eq. 12 of Ref. [8])

$$\psi_{ii} + \alpha\psi_i + \cos\varphi \sin\psi + \delta I_C \cos\psi \sin\varphi = -\frac{2}{\beta_l} \left(\psi - \pi \frac{\Phi_c}{\Phi_0} \right),$$

where $\delta I_C = (I_{C1} - I_{C2})/2I_C$, $I_C = (I_{C1} + I_{C2})/2$ and $\beta_l = (2\pi I_C)/\Phi_0$. From this equation, following a linear expansion for the static limit performed for small β_l and assuming a small δI_C , a single equation for the variable φ (analogous of Eq. 16 of Ref. [8]) and related potential energy (1) can be derived.

Given a particular experimental configuration, the four energies introduced above can be modulated by varying the two fluxes coupled to the system (Φ_x and Φ_c). The difference between the Josephson currents of the junctions of the inner loop, related to the third term in Eq. (1), can be due to either fabrication parameter uncertainties or flux trapping in the junctions or it can be imposed deliberately through the design of the chips. The stable and metastable states of the variable $\Phi = (\Phi_0/2\pi)\varphi$ can be displayed versus the control fluxes Φ_x and Φ_c as shown in Fig. 4(a). The surface shown in the figure is a known feature of Thom's catastrophe theory [9–11] and, in the jargon of this theory, it is

called the behavior surface of the system. The surface is analytically determined by the fix points of the system described by Eq. (1); i.e., the zero point of the first derivative of Eq. (1):

$$\varphi_x = \varphi + \frac{E_S}{E_L} \sin\varphi + \frac{E_D}{E_L} \cos\varphi + \frac{E_l}{E_L} \sin\varphi \cos\varphi. \quad (2)$$

The fold in the surface of Fig. 4(a) maps discontinuous transitions between multiple states that occur due to a change in a variable. The critical point at which a catastrophe occurs (i.e., a discontinuous transition from one point to another on a folded surface) corresponds to a point where a minimum and a maximum coincide. These values can be determined from the two conditions $\partial U/\partial\varphi = 0$ and $\partial^2 U/\partial\varphi^2 = 0$, which yield the critical value of φ_x . For fixed values of other parameters contributing to E_S , E_D , E_l , E_L we thereby obtain plots of the critical points in the Φ_x - Φ_c plane, as shown in Figs. 4(b)–4(d).

Equation (1) can be readily transformed into the polynomial form analyzed by Thom [9–11] for the butterfly catastrophe by approximating the energy expression with a sixth order polynomial Taylor expansion around the point $\varphi = \pi$ (corresponding to $\Phi = \Phi_0/2$); removing the constant term and retaining only the leading power in the terms having the same coefficients we get

$$U = \frac{(\varphi - \pi)^6}{60} E_l - \frac{(\varphi - \pi)^4}{24} (4E_l - E_S) + \frac{(\varphi - \pi)^3}{6} E_D + \frac{(\varphi - \pi)^2}{2} (E_L + E_l - E_S) - \varphi(E_D + \varphi_x - \pi). \quad (3)$$

Thus, four physically relevant energies of our system directly determine the coefficients of the 6th order polynomial of the butterfly catastrophe. The phase diagrams shown in figures from 4(b) to 4(d) are related to three different sets of energy scales relevant for our experiment. The approximate potential in Eq. (3) (dashed lines) fits very well the full potential in Eq. (1) (solid lines). We note that when the energy stored in the inductor l can be neglected, and when there is no Josephson energy associated with the difference of the currents of the internal loop (the junctions are identical), the form (3) becomes a fourth order polynomial of the cusp catastrophe accounting for the behavior of the rf-SQUID. Equation (3) very clearly displays the relevance of the inductance l , which determines the coefficient to the term of highest order, as well as the sign of the fourth order term.

The important parameters that we get out of the fit are E_{S0}/E_L , E_{D0}/E_L and E_{l0}/E_L . From these quantities it is possible to determine all the system parameters I_{C1} , I_{C2} , and l once the inductance L is known (in our device we have a nominal inductance $L = 85$ pH). In Figs. 3(a) and 3(b) we show the theoretical curves fitting the data that were obtained with $E_{S0}/E_L = 4.9$, $E_{D0}/E_L = 0.196$, and $E_{l0}/E_L = 0.54$, corresponding to $l = 7.7$ pH, $(I_{C1} + I_{C2}) = 19.0$ μ A, and asymmetry $(I_{C1} - I_{C2})/(I_{C1} + I_{C2}) = E_{D0}/E_{S0} = 0.04$. These parameters are fully con-

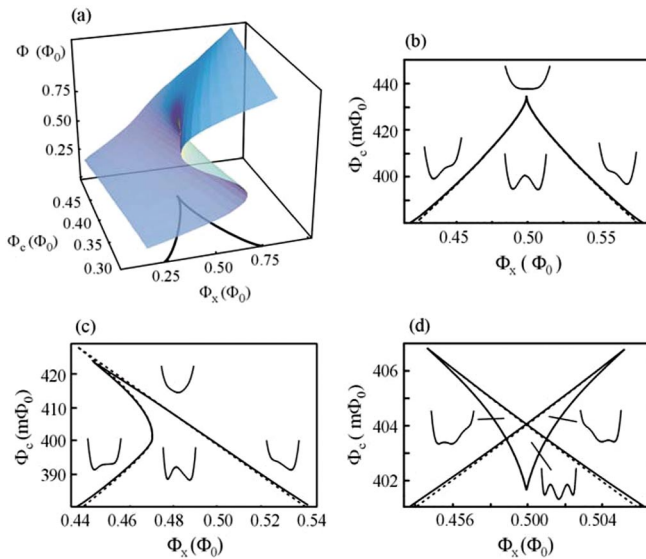


FIG. 4 (color online). (a) Characteristic surface described by possible phase solutions of a double-SQUID system. Shown surface is obtained by varying the two parameters that can be changed during measurements; this kind of surface represents a typical topological feature of systems exhibiting catastrophes. (b)–(d) Examples of parameter locations of catastrophes and sketch of the corresponding configurations of the potential [Eq. (3)]. (b) Parameter values identical to (a); (c) and (d) are projections of the surface for different parameter sets of the butterfly catastrophe. Solid and dashed curves are obtained by using, respectively, the full potential or a 6th order Taylor expansion.

sistent with the asymmetry value derived from the flux modulations, meaning that the potential model of Eq. (1) provides a realistic description of our system.

In Fig. 3(c) we further show that the experimental points fit the shape of the butterfly catastrophe that we obtain from Eq. (2) for small junctions asymmetry [corresponding to a coefficient of the third order power close to zero in Eq. (3)]. The theoretical curve is the typical butterfly catastrophe and is obtained for $E_{S0}/E_L = 5.2$, $E_{D0}/E_L = 0.0156$, and $E_{I0}/E_L = 0.61$, corresponding to $l = 7.7$ pH, $(I_{C1} + I_{C2}) = 20.1$ μ A, and $(I_{C1} - I_{C2})/(I_{C1} + I_{C2}) = E_{D0}/E_{S0} = 0.003$. The asymmetry is consistent with the estimate obtained from the flux modulations. It is worth noting that no evidence of either the tip bending shown in Figs. 3(a) and 3(b) or of the butterfly catastrophe shown in Fig. 3(b) was recorded at 4.2 K; the data shown in these figures were recorded at 10 mK. In terms of potential wells [see Fig. 4(d)] the butterfly implies that an extra potential well exists between the right and left wells: when the control parameters lead the system in the “pocket” of the butterfly [see Fig. 4(d)] we can clearly see that the potential develops this third and central well in which the current is circulating only in the small loop of our double-SQUID system.

From the coefficients of Eq. (3) it is straightforward to anticipate the behavior that we observed experimentally. The coefficient of the fourth order term in that equation can be conveniently modulated experimentally via the normalized flux Φ_c/Φ_0 . A particular feature of the experiments is that this coefficient is always negative, which is an important component for the butterfly catastrophe surface. Also, the coefficient regulating the shape of the tip is the third order term, namely E_D : when this term is close to zero we find experimentally the symmetrical projection of the butterfly singularity, just as predicted by the topological model [9–11]. An interesting analysis related to the butterfly catastrophe was reported for a three level optical system [12].

Because of the presence of the three-well structure in the sample considered in this Letter, performing quantum coherence experiments according to our initial idea is a nontrivial task. However, simulation shows that, with a slight modification of the parameter values (for instance, a reduction of the critical current by about 15%), the third well disappears in the operational region and the overall modification of the potential profile is reduced to a small perturbation. Thus, an adequate design of the SQUID system should allow recovering the original measurement scheme.

In conclusion, our characterization of a double-SQUID potential has shown that small deviations from ideal conditions have profound impacts on the shape of the potential energy. We have shown that the modification of the potential can be explained in terms of the general nonlinear system analysis introduced by Thom: namely, catastrophe theory. The theoretical description of our experimental

results obtained according to this model is accurate and consistent with independent parameter evaluations. We believe that quantum coherence experiments based on the Josephson flux variable can benefit from the analysis and the characterization of the potential that we have presented herein.

The chips used for the experiments, made in a standard Nb trilayer technology [13], were fabricated by Hypres Inc, NJ (USA). We wish to thank Professor R. de Bruyn Ouboter for enthusiastic encouragement. The work was partially supported by INFN (Italy), by European Community Project RSFQubit (No. FP6-3748), by a No. MIUR-COFIN04 (Italy) and by a No. MIUR-FIRB03 (Italy). Partial support by AFOSR Grant No. FA9550-04-1-0711 through the Center for Digital Security, UC Davis (USA) is also acknowledged.

-
- [1] A. J. Leggett and A. Garg, *Phys. Rev. Lett.* **54**, 857 (1985).
 - [2] M. H. Devoret, J. M. Martinis, and J. Clarke, *Phys. Rev. Lett.* **55**, 1908 (1985); P. Silvestrini, V. G. Palmieri, B. Ruggiero, and M. Russo, *Phys. Rev. Lett.* **79**, 3046 (1997); J. M. Martinis, S. Nam, J. Aumentado, and C. Urbina, *Phys. Rev. Lett.* **89**, 117901 (2002); A. Wallraff, T. Duty, A. Lukashenko, and A. V. Ustinov, *Phys. Rev. Lett.* **90**, 037003 (2003).
 - [3] F. W. Strauch, P. R. Johnson, A. J. Dragt, C. J. Lobb, J. R. Anderson, and F. C. Wellstood, *Phys. Rev. Lett.* **91**, 167005 (2003).
 - [4] J. R. Friedman, V. Patel, W. Chen, S. K. Tolpygo, and J. E. Lukens, *Nature (London)* **406**, 43 (2000); M. Cirillo *et al.*, *Physica (Amsterdam)* **C437–438**, 46 (2006).
 - [5] I. Chiorescu *et al.*, *Science* **299**, 1869 (2003); J. Claudon *et al.*, *Phys. Rev. Lett.* **93**, 187003 (2004); R. McDermott *et al.*, *Science* **307**, 1299 (2005); R. H. Koch *et al.*, *Phys. Rev. Lett.* **96**, 127001 (2006).
 - [6] C. Cosmelli *et al.*, *IEEE Trans. Appl. Supercond.* **15**, 849 (2005).
 - [7] A. Barone and G. Paternò, *Physics and Applications of the Josephson Effect* (J. Wiley, NY, 1982); T. Van Duzer and C. W. Turner, *Principles of Superconductive Devices and Circuits* (Elsevier, NY, 1998).
 - [8] N. Grønbech-Jensen, D. B. Thompson, M. Cirillo, and C. Cosmelli, *Phys. Rev. B* **67**, 224505 (2003).
 - [9] R. Thom, *Structural Stability and Morphogenesis* (Benjamin, Reading, MA, 1975).
 - [10] E. C. Zeeman, in *Lectures on Mathematics in the Life Sciences*, edited by Simon A. Levin, *Some Mathematical Questions in Biology Vol. 7* (American Mathematical Society, Providence, 1974).
 - [11] P. T. Saunders, *An Introduction to Catastrophe Theory* (Cambridge University Press, Cambridge, England, 1980); R. Gilmore, *Catastrophe Theory for Scientists and Engineers* (Dover, New York, 1981).
 - [12] M. Kitano, T. Yabukazi, and T. Ogawa, *Phys. Rev. Lett.* **46**, 926 (1981).
 - [13] S. Morohashi and S. Hasuo, *J. Appl. Phys.* **61**, 4835 (1987).